Since January 2020 Elsevier has created a COVID-19 resource centre with free information in English and Mandarin on the novel coronavirus COVID-19. The COVID-19 resource centre is hosted on Elsevier Connect, the company's public news and information website.

Expert Systems With Applications 213 (2023) 119206

Contents lists available at ScienceDirect

Expert Systems With Applications

journal homepage: www.elsevier.com/locate/eswa

Improved deep convolutional neural networks using chimp optimization algorithm for Covid19 diagnosis from the X-ray images

Chengfeng Cai [a], Bingchen Gou [a,*], Mohammad Khishe [b], Mokhtar Mohammadi [c], Shima Rashidi [d], Reza Moradpour [b], Seyedali Mirjalili [e,f]

[a] School of Mechanical Engineering, Northwestern Polytechnical University, Xi'an 710072, China
[b] Departement of Electrical Engineering, Imam Khomeini Marine Science University, Nowshahr, Iran
[c] Department of Information Technology, College of Engineering and Computer Science, Lebanese French University, Kurdistan Region, Iraq
[d] Department of Computer Science, College of Science and Technology, University of Human Development, Sulaymaniyah, Kurdistan Region, Iraq
[e] Centre for Artificial Intelligence Research and Optimization, Torrens University, Australia
[f] University Research and Innovation Center, Obuda University, 1034 Budapest, Hungary

ARTICLE INFO

Keywords:
Chimp Optimization Algorithm
COVID-19 diagnosis
Deep learning
Convolutional neural networks
Chest X-rays
Machine learning

ABSTRACT

Applying Deep Learning (DL) in radiological images (i.e., chest X-rays) is emerging because of the necessity of having accurate and fast COVID-19 detectors. Deep Convolutional Neural Networks (DCNN) have been typically used as robust COVID-19 positive case detectors in these approaches. Such DCCNs tend to utilize Gradient Descent-Based (GDB) algorithms as the last fully-connected layers' trainers. Although GDB training algorithms have simple structures and fast convergence rates for cases with large training samples, they suffer from the manual tuning of numerous parameters, getting stuck in local minima, large training samples set requirements, and inherently sequential procedures. It is exceedingly challenging to parallelize them with Graphics Processing Units (GPU). Consequently, the Chimp Optimization Algorithm (ChOA) is presented for training the DCNN's fully connected layers in light of the scarcity of a big COVID-19 training dataset and for the purpose of developing a fast COVID-19 detector with the capability of parallel implementation. In addition, two publicly accessible datasets termed COVID-Xray-5 k and COVIDetectioNet are used to benchmark the proposed detector known as DCCN-Chimp. In order to make a fair comparison, two structures are proposed: i-6c-2 s-12c-2 s and i-8c-2 s-16c-2 s, all of which have had their hyperparameters fine-tuned. The outcomes are evaluated in comparison to standard DCNN, Hybrid DCNN plus Genetic Algorithm (DCNN-GA), and Matched Subspace classifier with Adaptive Dictionaries (MSAD). Due to the large variation in results, we employ a weighted average of the ensemble of ten trained DCNN-ChOA, with the validation accuracy of the weights being used to determine the final weights. The validation accuracy for the mixed ensemble DCNN-ChOA is 99.11%. LeNet-5 DCNN's ensemble detection accuracy on COVID-19 is 84.58%. Comparatively, the suggested DCNN-ChOA yields over 99.11% accurate detection with a false alarm rate of less than 0.89%. The outcomes show that the DCCN-Chimp can deliver noticeably superior results than the comparable detectors. The Class Activation Map (CAM) is another tool used in this study to identify probable COVID-19-infected areas. Results show that highlighted regions are completely connected with clinical outcomes, which has been verified by experts.

1. Introduction

Early diagnosis of COVID-19 positive cases is essential to keep the infected person isolated and lower the risk of spreading the virus to others in the community (Zhaowei Zhang et al., 2022b). Blood samples, respiratory gene sequences, and reverse transcription-polymerase chain reactions (RT-PCR) have all been suggested as the three main screening modalities for COVID-19 (Zhuo et al., 2020). On the other hand, it is reported that between 30 % and 60 % of throat swab cases are positive on the RT-PCR test, meaning that many healthy persons are infected by patients who go untreated. Because of its convenience and speed, chest radiography imaging (including CT and X-ray pictures) is a common technique for diagnosing pneumonia. The fundamental flaw of chest CT has been demonstrated to be its high sensitivity for COVID-19 diagnosis,

* Corresponding author.
E-mail addresses: goubingchen@hotmail.com (B. Gou), m_khishe@alumni.iust.ac.ir (M. Khishe), shima-Rasshid@edu.krd (S. Rashidi).

https://doi.org/10.1016/j.eswa.2022.119206
Received 12 August 2021; Received in revised form 17 September 2022; Accepted 31 October 2022
Available online 4 November 2022

Table 1
The detailed information for the resources datasets.

Dataset	COVID-19	Pneumonia	Normal	Total
Source datasets				
COVID-19 Radiography Database[1]	219	1345	1341	2905
covid-chestxray-dataset[2]	76	17	–	93
Pneumonia[3]	–	4273	1583	5856
Used datasets				
COVIDetectioNet	219	4290	1583	6092
COVID-X-ray-5 k	520	–	5000	5520

[1] https://https://www.kaggle.com/tawsifurrahman/covid19-radiography-database.
[2] https://github.com/tawsifur/COVID-19-Chest-X-ray-Detection.
[3] https://https://www.kaggle.com/paultimothymooney/chest-xray-pneumonia.

Table 2
The combination of photos in different datasets.

Category	Normal	COVID19
	COVID-X-ray-5 k	
Training Set	2000	420 (84 before augmentation)
Test Set	3000	100
	COVIDetectioNet	
Training Set	2873	150
Test Set	3000	69
Total		
Training Set	4873	570
Test Set	6000	169

whereas COVID-19-related visual indexes are visible on X-ray pictures (Nilashi et al., 2020).

It should be stated that peripheral airspace opacities and multi-lobar involvement are reported in chest imaging. In these cases, ground-glass and mixed consolidation (i.e., lobar and patchy) with 57 % and 29 % are the most frequently reported opacities. In the early stages of COVID-19, regions that border the pulmonary arteries can be seen to have a ground glass appearance; however, this kind of symptom is difficult to diagnose visually (K. Zhang et al., 2021). Clinical studies also report diffuse airspace or asymmetric patchy opacities as other frequent COVID-19 symptoms (Cao et al., 2022). It must be noted that only expert radiologists can interpret those mentioned subtle abnormalities (Jin et al., 2022; Xu et al., 2020). Because of the high volume of suspicious cases and the scarcity of qualified radiologists, automatic diagnostic methods can assist radiologists in identifying such subtle abnormalities and increase the early diagnosis rate with high accuracy.

Considering the reliability (Liao et al., 2021), accuracy (Ban et al., 2022), buildability (Zhu et al., 2022), easiness to use (Liao et al., 2021), stability (Luo et al., 2022a; Luo et al., 2022b), machine learning and deep learning techniques are two effective solutions for addressing these image processing issues (J. Li et al., 2022; Y. Zhang et al., 2022a; Zhao & Wang, 2022); therefore, a reliable dataset is absolutely necessary to have an authentic experiment (Y. Li et al., 2021; Liao et al., 2021). Recently, several X-ray Covid 19 datasets have been presented by researchers. Despite the usefulness of this data set for artificial intelligence specialists, they have not been approved by board-certificate radiologists. Researchers extract these images from research papers reporting the COVID-19 studies based on CT and X-ray images. However, for the sake of having an authentic experiment and keeping the power of sample size, we use COVID-Xray-5 k (Minaee et al., 2020) and the *COVIDetectioNet* dataset (Turkoglu, 2021), in which a trained radiologist changed the labels on the X-rays so that only the ones showing evidence of the COVID-19 would be retained.

As the requirement of introducing an accurate and fast detector and considering DL's remarkable capability in this application (Mohammad Khishe et al., 2021; Pan et al., 2020; Wu et al., 2021), this paper proposes to use DCNN as a COVID-19 detector. Since the beginning of 2020, some research papers have been conducted to develop models to recognize positive Covid-19 cases (Arnal et al., 2020; Hu et al., 2021a; Rodriguez et al., 2020; K. Zhang et al., 2021).

To overcome the aforementioned drawbacks, our proposed strategy involves training a DCNN from a draft on Data 1; then, the final fully-connected layer of the pre-trained DCNN is substituted with a new fully-connected layer that has been fine-tuned by the ChOA (M. Khishe & Mosavi, 2020). In this case, a specific network structure will be proposed by Chimps.

The main contributions of this paper are as follows:

- An end-to-end nature-inspired DCNN is provided to effectively diagnosis COVID-19-positive cases.
- The chimp Optimization Algorithm is used for the first time in this paper to tune the DCNN's parameters.
- The proposed method's parallel structure causes its easy implementation on the GPU substrate.
- Detailed experimental analysis of the models' performance in terms of specificity, sensitivity, Receiver Operating Characteristic (ROC), and the precision-recall curves is provided.
- The paper also exploits the CAM concept to detect the areas probably infected by the Covid-19 virus.

The remainder of the paper is structured as follows. In Section 2, mostly related research works are reviewed. Background materials, including DCNN, ChOA, and COVID19-X-ray datasets, are presented in Section 3. Section 4 introduces the proposed ChOA fine-tuning scheme. Section 5 represents the simulation results and discussion, and conclusions are finally described in Section 6.

2. Related works

The early identification and diagnosis of COVID19-positive patients and other difficult image detection and analysis tasks have benefited from the use of DL models. Deep-COVID was nearly the first to use DL models to identify COVID19. SqueezeNet, ResNet18, SqueeezeNet, ResNet50, and DenseNet-121, four well-known DCNNs, were suggested to detect COVID19-positive patients in the studied chest X-ray photos in this research. There is a unique dataset (COVID-Xray-5 k) that clinicians confirmed in the reference (Minaee et al., 2020). We chose this dataset because of its unique character as a benchmark.

An autonomous DarkNet system was demonstrated to be able to categorize items into multiclass and binary categories in reference (Ozturk et al., 2020). Although this model included Seventeen convolution layer and several filtering on each layer, which made it fairly complex, it was intended to achieve accuracy of up to 98 percent. A special DCNN called CoroNet (A. I. Khan et al., 2020) was proposed to automatically identify COVID19-positive individuals from chest X-ray images. CoroNet was developed utilizing the COVID19 and other pulmonary pneumonia X-ray images from two other publicly accessible sources after training on the ImageNet dataset. Despite the proposed model being straightforward and effective, the accuracy and dependability of the results were satisfactory. Reference (Wang et al., 2020) advocated using a COVID-Net DCNN to detect COVID19-positive instances. The X-ray imagery of the chest was divided into two categories using this model: normal and COVID19. Two publicly accessible datasets were used to evaluate the performance of the COVID-Net model. COVID-Net had the greatest average accuracy of 92.4 percent, which is not at all remarkable. COVIDX-Net (Hemdan et al., 2020) is a DL model designed to diagnose COVID19-positive individuals by analyzing chest X-ray images. A new dataset of fifty X-ray images was used to test this model against several well-known pre-trained models, including DenseNet201

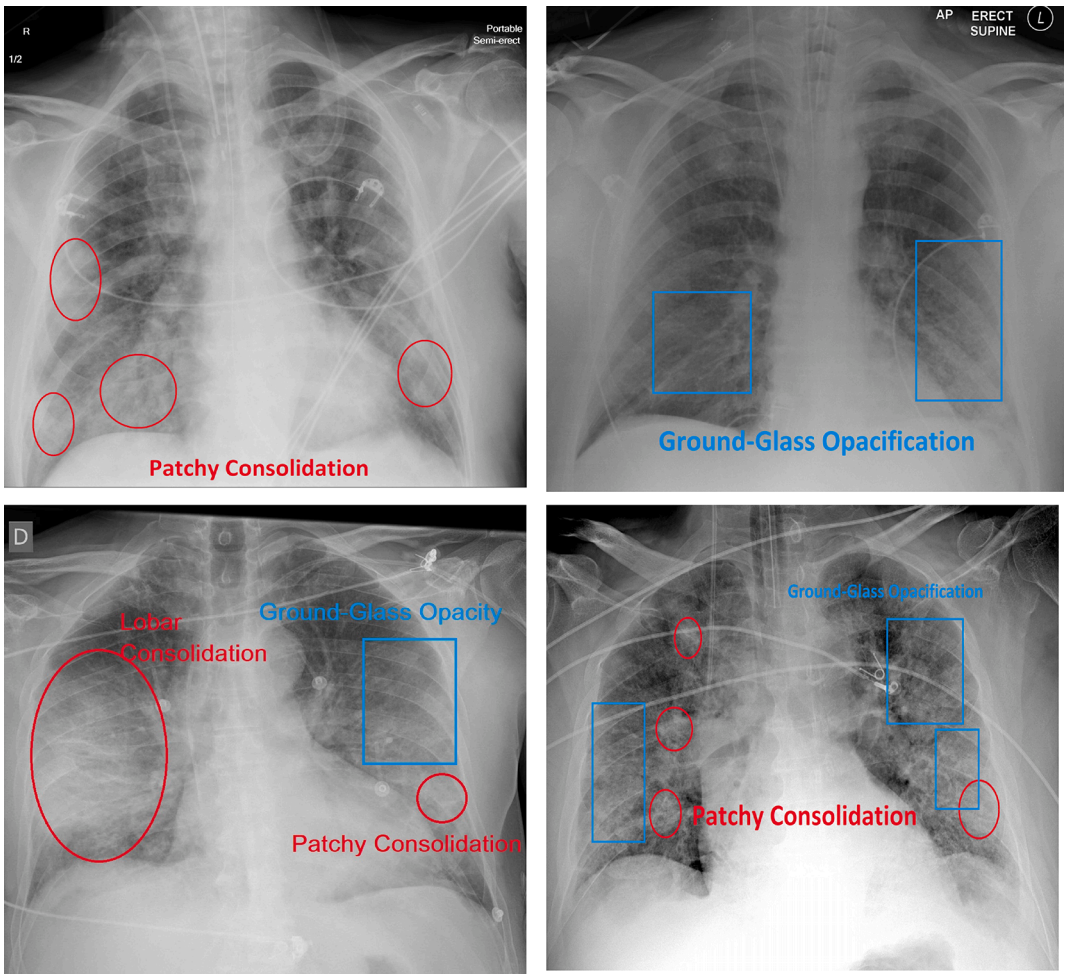

Fig. 1. Typical Chest X-ray images, showing ground-glass opacification (blue rectangles) as well as lobar and patchy consolidation (red ellipses).

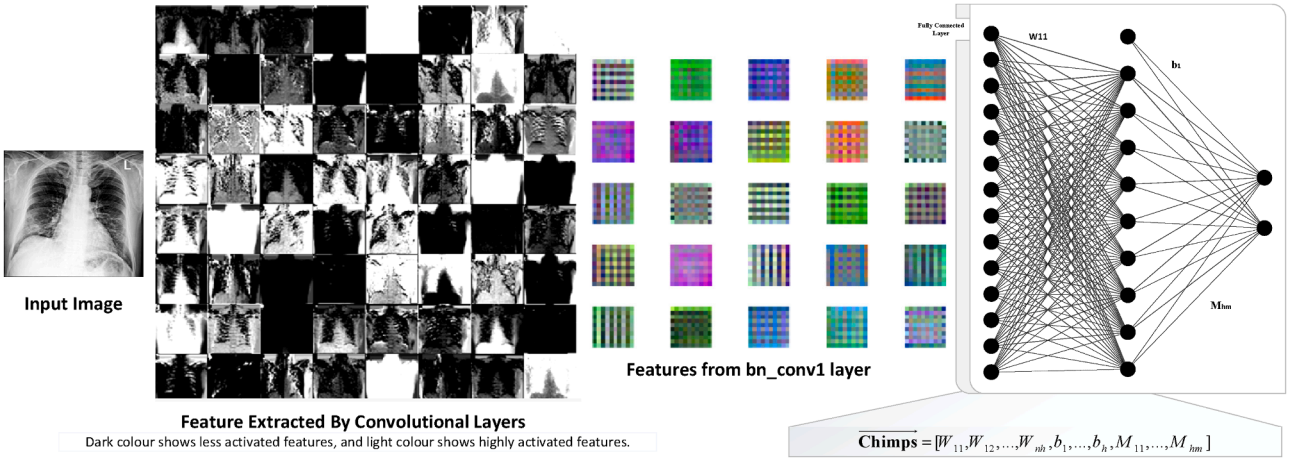

Fig. 2. Allocating the parameters of DCNN as the chimps (candid solutions) of ChOA.

and VGG19. The DenseNet201 had the best accuracy (91 percent) in this trial. Using the Entropy technique and twelve ML algorithms, reference (Mohammed et al., 2020) suggested a unique approach for selecting the optimal COVID19 detector. The linear SVM model was the most accurate, with a 98.99 percent accuracy rate. The model had a very high level of spatial and temporal complexity despite having great classification accuracy.

The input image was converted into lower-dimensional retrieved features using DCNNs as feature extractors as well (Hu et al., 2021b; Lu et al., 2022). In order to arrive at the final choice, these output feature vectors were put into a variety of classification algorithms (Feng et al., 2022). Manual parameter setup and matching of feature extraction and classifier sections are required despite the approaches' high classification accuracy (98–99 %). In addition, the final model's complexity is rather significant (Dai et al., 2022).

Classifier performance may be improved by using preprocessing

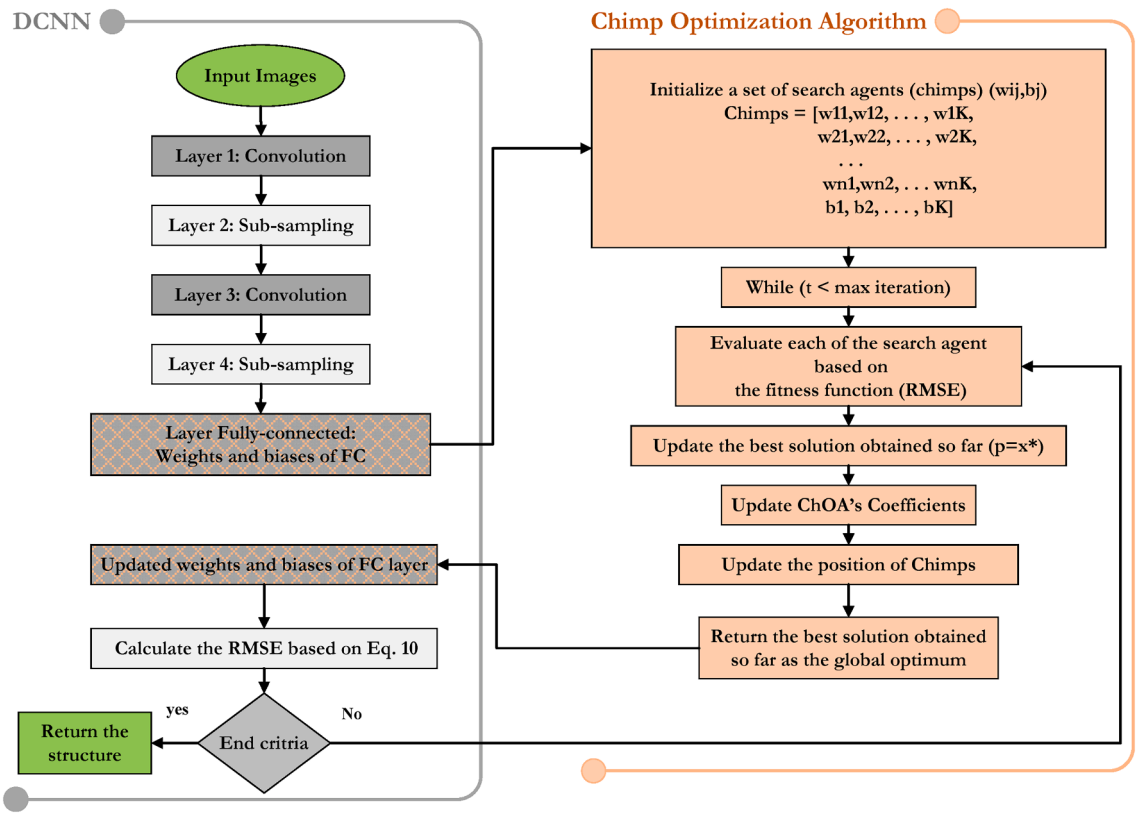

Fig. 3. The flowchart for the DCNN-ChOA.

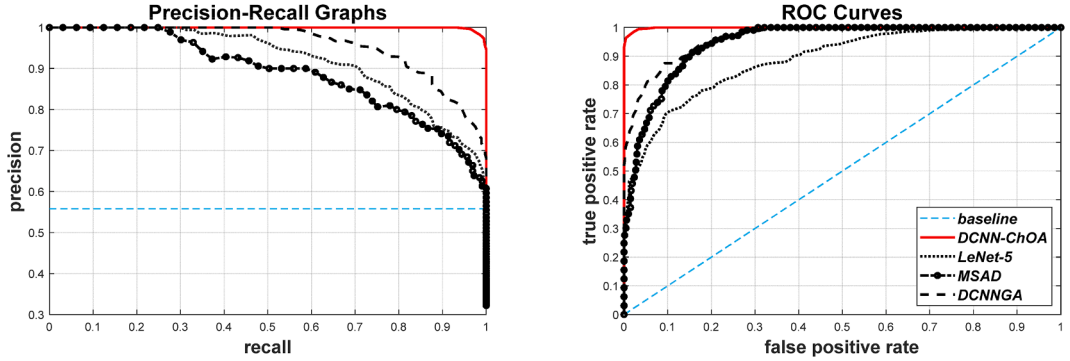

a) i-6c-2s-12c-2s model.

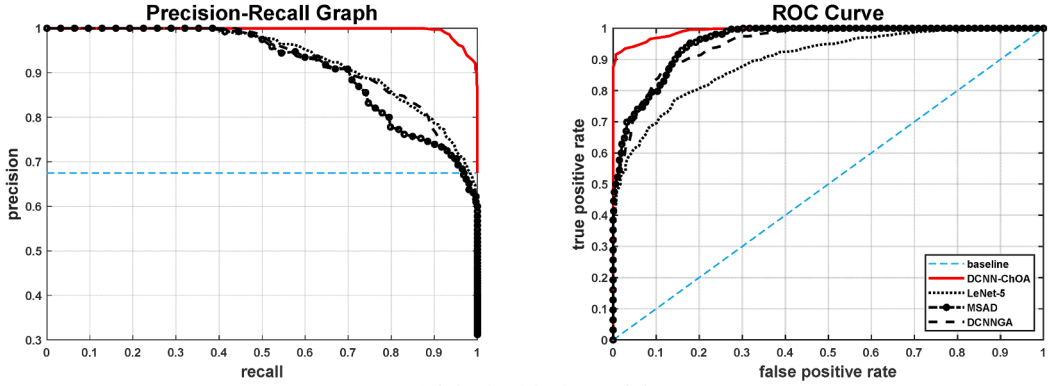

b) i-8c-2s-16c-2s model.

Fig. 4. Precision-recall and ROC curves.

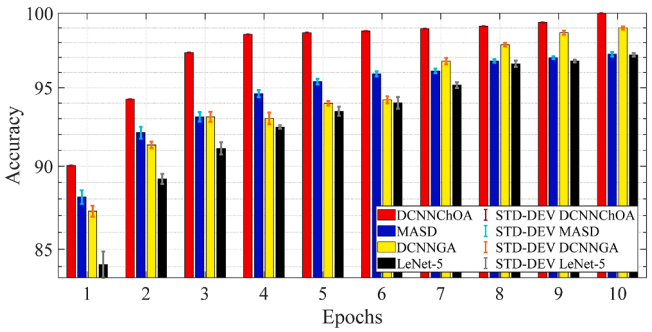

Fig. 5. Accuracy and STD for the i-2 s-6c-2 s-12c structure.

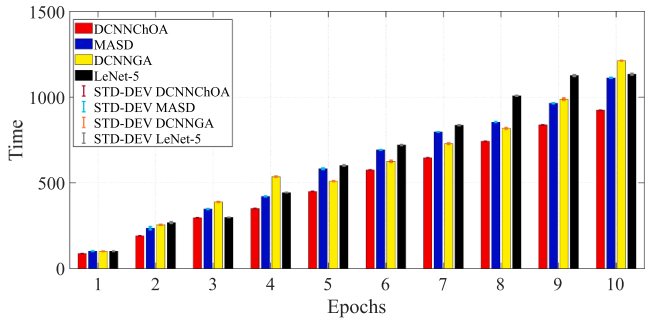

Fig. 6. Computation time for the i-2 s-6c-2 s-12c structure.

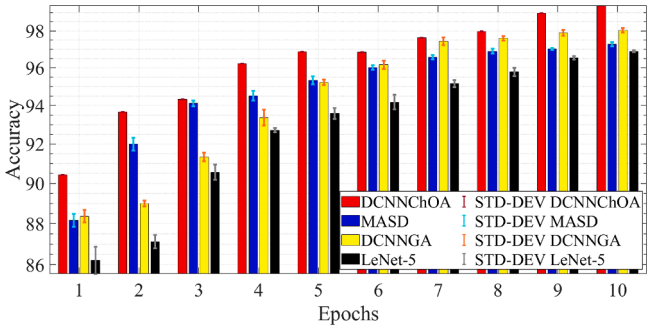

Fig. 7. Accuracy and STD for the i-2 s-8c-2 s-16c structure.

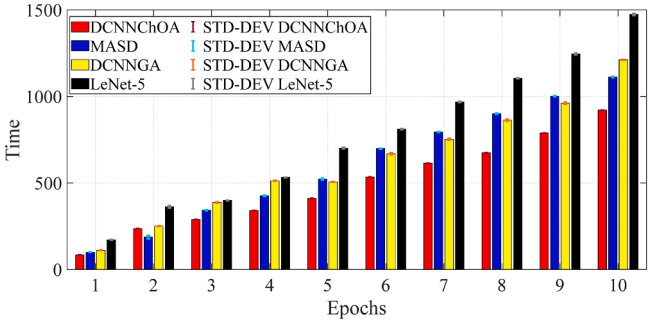

Fig. 8. Computation time for the i-2 s-8c-2 s-16c structure.

approaches, on the other hand (Xie et al., 2022; Zhou et al., 2019). Three preprocessed images were produced by researchers (Heidari et al., 2021) using preprocessing techniques such diaphragm removal and adjusting image contrast. These images were then applied to a transfer learning technique (i.e., VGG16) to categorize chest X-ray images into three

Table 7
The comparison of the DCNN-ChOA and other DL models, which have used the *COVID-Xray-5 k* dataset.

No.	model	Sensitivity (%)	Specificity (%)	Accuracy (%)
1	ResNet18 (Minaee et al., 2020)	98	90.7	–
2	ResNet50 (Minaee et al., 2020)	98	89.6	–
3	SqueezeNet (Ucar & Korkmaz, 2020)	98	92.9	–
4	DenseNet-121 (Sarker et al., 2020)	98	75.1	–
5	ResNet-101 (Tahir et al., 2021)	77.3	71.8	71.9
6	CB-STMRENet (Che Azemin et al., 2020)	–	–	93
7	VGG16 (I. U. Khan & Aslam, 2020)	99.28	99.38	99.33
8	VGG19 (I. U. Khan & Aslam, 2020)	100.00	98.78	99.33
9	OptiCNN (Mohammad Khishe et al., 2021)	–	–	99.11
10	CNN (Ahammed et al., 2020)	94.03	97.01	94.03
11	Deep Decision Tree (Yoo et al., 2020)	–	–	95
12	Support Vector Machine (Yoo et al., 2020)	–	–	96
13	K-Nearest Neighbors (Iwendi et al., 2020)	–	–	92
14	Random Forest (Iwendi et al., 2020)	–	–	92
15	Naïve Bayes algorithm (Mansour et al., 2021)	–	–	90
16	Decision Tree (Yoo et al., 2020)	–	–	82
17	Our i-2 s-8c-2 s-12c model	–	–	99.38
18	Our i-2 s-8c-2 s-16c model	–	–	100.00

categories: normal, pneumonia, and COVID-19. This machine learning technique was able to get a classification accuracy of 93,9%. A binary classifier was developed by comparing Inception V2, VGG-19, and the clustering algorithm (Dansana et al., 2020). Images with a high degree of noise were reduced by employing a features extraction kernel to build compact feature maps. The DL models used these feature maps as input. Inception V2 had a 60 % accuracy rate, while the decision tree approach had a 91 % accuracy rating, with VGG-19 coming in second with a 78 % accuracy rate. Prior to using a preprocessing approach to identify and remove diaphragm regions from photos, a bilateral filter and histogram equalization technique are used to create two groups of filtered images (Heidari et al., 2020). With these three photos as inputs, we can improve the depth of our DCNN model's learning capabilities by adding even more data to it. These methods may improve the performance, but they will almost certainly increase the overall system's complexity.

There are many learning problems that can be solved using DL due to its impressive properties, however training is difficult (Afrakhteh et al., 2020; M. R. Mosavi et al., 2017a; Mohammad Reza Mosavi et al., 2017b). By reviewing the literature, it can be realized that eminent algorithms for training DL are GD (Afrakhteh et al., 2020), CG (Shewchuk, 1994), HFO (Martens, 2010; Yin et al., 2021), and KSD (Vinyals & Povey, 2012). GDB techniques require extensive manual parameter adjustment for best performance. Their sequential design makes it difficult to parallelize them using GPUs. However, despite being stable for training, CG approaches are also incredibly sluggish, requiring numerous CPUs and a lot of memory (Zhenhao Zhang et al., 2020). HFO was used to train the weights of a conventional CNN by deep auto-encoders (Martens, 2010), and this method is more efficient for the fine-tuning of deep auto-encoders than the model developed by reference (Hinton & Salakhutdinov, 2006). In addition, KSD is less complicated and more stable than HFO. As a result, it offers faster

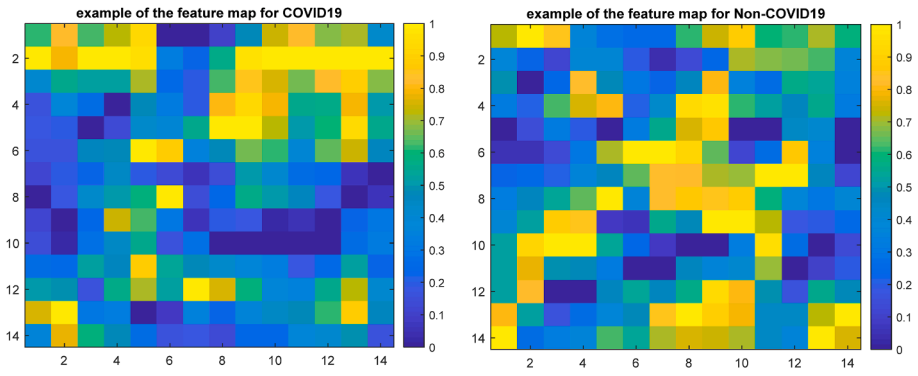

(a) COVID19 (b) Non-COVID19

Fig. 9. An illustration of a feature map, (a) COVID19 and (b) Non-COVID19.

optimization and classification rates than HFO. On the other hand, KSD has higher memory requirements than HFO.

Recently, evolutionary and metaheuristic algorithms have been widely applied to optimize different engineering optimization tasks (M. Khishe & Mosavi, 2019; Qiao et al., 2021). The hybrid GA and DCNN model described in (Chhikara et al., 2020) was the first study to employ metaheuristic optimization techniques for this type of optimization model. The Harmony Search (HS) technique was proposed by Rosa et al. (Rosa et al., 2015) as an evolutionary fine-tuning strategy for maximizing the DCNN's potential.

A PUL is introduced by (Fan et al., 2018) to utilize pre-trained DCNN. An automatic DCNN architecture using GA is introduced by (Fan et al., 2018) to optimize image classification problems. Nevertheless, this automatic GA-based method's primary shortcoming is that large DCNNs cause GA to slow down as its chromosomes grow too large. Other popular research works in this field are improved evolutionary clustering algorithm star (Hassan et al., 2021), hybrid genetic algorithm and machine learning method (Zivkovic et al., 2021), and hybrid Gabor filter and convolutional deep learning classification method (Barshooi & Amirkhani, 2022).

3. Background materials

The background information, including the COVID-X-ray datasets, the DCCN model, and ChOA, is presented in this section.

3.1. The mathematical model of ChOA

The ChOA is an innovative optimization technique that takes inspiration from the chimpanzees' foraging behavior. There are four different kinds of chimps in their community: drivers, chasers, barriers, and attackers. Following are main mathematical models of ChOA (M. Khishe & Mosavi, 2020):

$$\boldsymbol{LOC}_{chimp}(k+1) = \boldsymbol{LOC}_{\text{prey}}(t) - \boldsymbol{b}\cdot\left|\boldsymbol{d}\cdot\boldsymbol{LOC}_{\text{prey}}(k) - \boldsymbol{ch}\cdot\boldsymbol{LOC}_{chimp}(k)\right| \quad (1)$$

$$\boldsymbol{b} = 2\cdot\boldsymbol{N}\cdot\boldsymbol{r}_1 - \boldsymbol{N} \quad (2)$$

$$\boldsymbol{d} = 2\boldsymbol{r}_2 \quad (3)$$

$$ch = \text{Chaotic} - \text{vector} \quad (4)$$

Where k denotes the number of iterations, $\boldsymbol{LOC}_{chimp}$ is the best location for the chimpanzee, $\boldsymbol{LOC}_{\text{prey}}$ is the best location (solution) so far, and **d**, **b**, and **ch** denote the coefficients' vectors. Additionally, r_1 and r_2 are randomly chosen values in the range (0,1], and **N** is a vector that is non-linearly decreased from 2.5 to 0 during the iterations; **ch** is a vector created from a number of chaotic mappings.

The most effective chimpanzees are used as prey in order to quantitatively replicate chimpanzee behavior because it is uncertain where the first prey was situated in the environment. As a result, additional individuals will be required to migrate proportionally to the new locations of the top four chimps, which ChOA will maintain according to the Eqs. (5) and (6).

$$\boldsymbol{LOC}(k+1) = \frac{1}{4}\times(\boldsymbol{LOC}_1 + \boldsymbol{LOC}_2 + \boldsymbol{LOC}_3 + \boldsymbol{LOC}_4) \quad (5)$$

Where

$$\begin{aligned}\boldsymbol{LOC}_1 &= \boldsymbol{LOC}_{Attacker} - \boldsymbol{b}_1.\left|\boldsymbol{d}_1\cdot\boldsymbol{LOC}_{Attacker} - \boldsymbol{ch}_1\cdot\boldsymbol{LOC}\right|\\ \boldsymbol{LOC}_2 &= \boldsymbol{LOC}_{Barrier} - \boldsymbol{b}_2.\left|\boldsymbol{d}_2\cdot\boldsymbol{LOC}_{Barrier} - \boldsymbol{ch}_2\cdot\boldsymbol{LOC}\right|\\ \boldsymbol{LOC}_3 &= \boldsymbol{LOC}_{Chaser} - \boldsymbol{b}_3.\left|\boldsymbol{d}_3\cdot\boldsymbol{LOC}_{Chaser} - \boldsymbol{ch}_3\cdot\boldsymbol{LOC}\right|\\ \boldsymbol{LOC}_4 &= \boldsymbol{LOC}_{Driver} - \boldsymbol{b}_4.\left|\boldsymbol{d}_4\cdot\boldsymbol{LOC}_{Driver} - \boldsymbol{ch}_4\cdot\boldsymbol{LOC}\right|\end{aligned} \quad (6)$$

As shown by Eq. (7), chaotic values can be used to imitate traditional ChOA social motivational behavior.

$$\boldsymbol{LOC}_{chimp}(k+1) = \begin{cases}\text{Eq. (5)}\ \lambda_m < 0.5\\ \boldsymbol{Chaotic - value}\ \lambda_m \geqslant 0.5\end{cases} \quad (7)$$

where λ_m stands for a random number between (0, 1]. An immature or gradual convergence rate may occur from the use of such a condensed learning model.

3.2. Convolution neural network

DCNNs are a type of neural network used most frequently in deep learning to evaluate visual data. DCNNs are sometimes referred to as Shifting Invariant or Spatial Invariant neural networks (LeCun, 2015). These ideas are organized by DCCNs into two main groups of layers, such as the pooling (sub-sampling) and convolution layers. The connection weights $\theta^k\psi$ and biases $\varphi_k\psi$generate the k_{th} fearture map (FEMA) $FEMA_{ij}^k$ using the *tanh* function, which is defined by Eq. (10) (LeCun, 2015).

$$FEMA_{ij}^k = \tanh((\theta^k \times x)_{ij} + \varphi_k) \quad (10)$$

The sub-sampling layer produces spatial invariance by lowering the resolution of FEMAs, where each FEMA corresponds to the FEMA of the preceding layer. Eq. (11) is used to define the pooling mechanism (LeCun, 2015).

$$\psi_j = \tanh(W\sum_{N\times N}\psi_i^{n\times n} + \omega) \quad (11)$$

Where $\psi_i^{n\times n}$ denotes the inputs,W and ω are trainable scalar and bias, respectively.

3.3. COVID-X-ray datasets

It was hypothesized that COVID-19′s sensitivity would be similar to

(a) COVID19

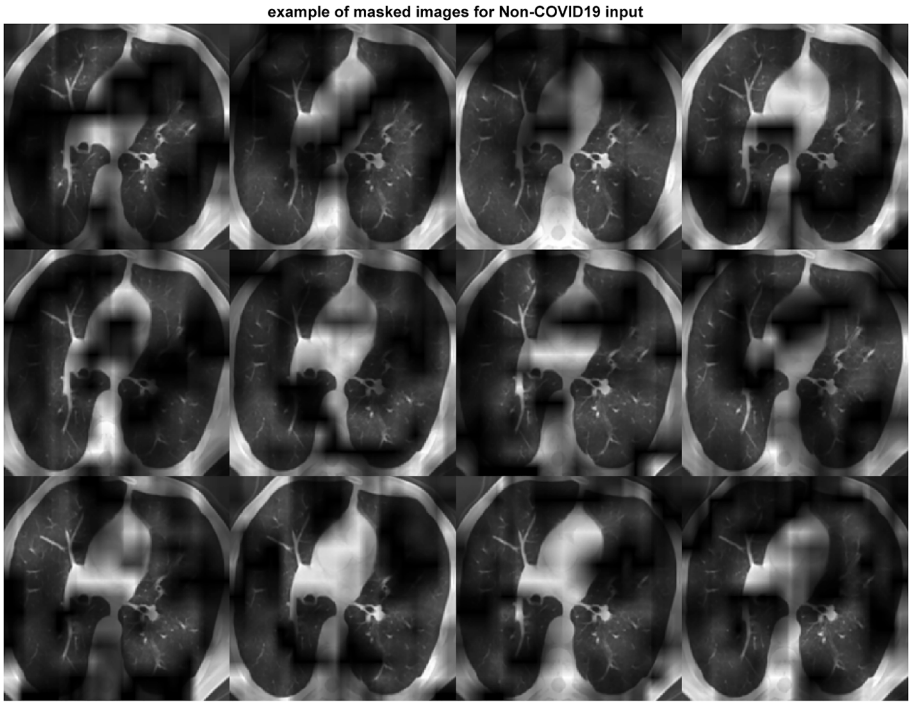

(b) Non-COVID19

Fig. 10. Typical example of masked images.

that of chest X-rays (56 %), based on the lower confidence range for X-ray sensitivity stated in reference (Wong et al., 2020). The required sample size was determined by multiplying the desired level of sensitivity (56 %) with the desired level of specificity (0.05) to get an overall power of 80 %. As a result, we calculated that there were around 165 individuals in the both positive and negative groups (a total of 330 sample).

In order to have enough test samples, this paper exploits two chest X-ray datasets to investigate the performance of the proposed model. The first utilized dataset is called COVID X-ray-5 k (Minaee et al., 2020). The COVID X-ray-5 k comprises of 3,100 testing set and 2,084 training set from two datasets of X-ray images. The initial dataset, known as Covid-Chestxray, was compiled by reference (Cohen et al., 2020) and included both chest X-ray and CT-scans COVID-19 images. There are 250 COVID-19 X-ray images in this dataset, 203 of which are anterior-posterior views. Additionally, it contains some *meta*-data about each photo, such as the gender and age. Given the board-certified radiologist's advice, all COVID-19-positive cases were selected from anterior-

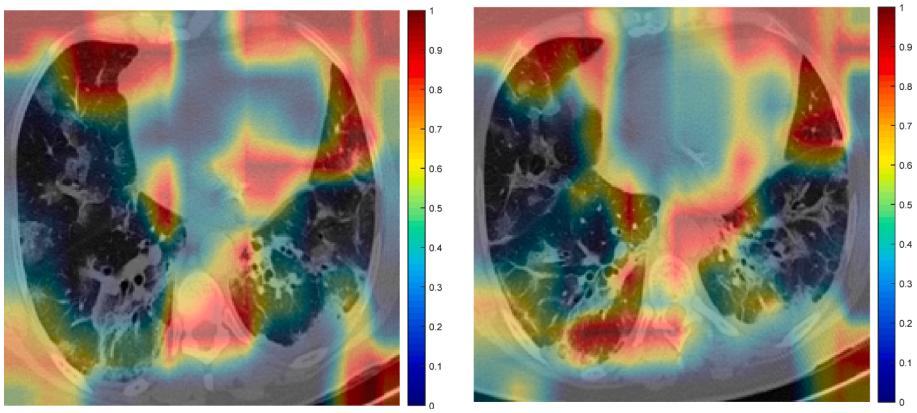

Fig. 11. The CAM demonstration for COVID19.

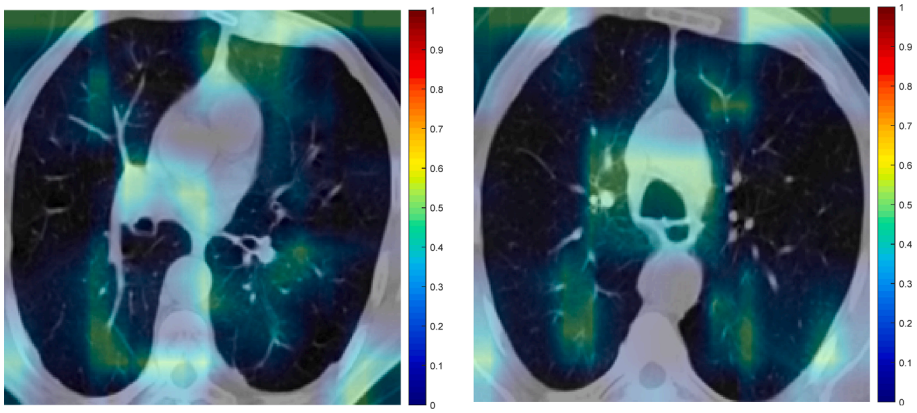

Fig. 12. The CAM demonstration for Non-COVID19.

posterior cases in this dataset. In the COVIDXray-5 k dataset, the board-certified radiologists investigated the anterior-posterior images to remove the images without the COVID-19 signs from the dataset. As a result, radiologists kept 184 images out of 203 interior-exterior X-rays with obvious signs of COVID-19 and eliminate 19 of them, of which their COVID-19 signs were not approved. This strategy introduced a new class with a more precisely classified dataset. In a total of 184 pictures, 100 are candidates for the test set, while the remaining 84 will serve as examples for the training set.

Data augmentation is used to bring the total number of confirmed cases up to 420. The additional ChexPert dataset (Irvin et al., 2019) was included as there were few normal instances in the covid-chestxray-dataset (Asif et al., 2020). This data set contains 224,316 images from 65,240 patients, organized into 14 subcategories (non-finding, Pneumonia, etc.). The 2,000 non-COVID photos used in the training set all came from the same category, with 700 coming from the non-finding sub-category and 100 from the other thirteen sub-categories. In conclusion, 2000 and 3000 non-COVID photos were selected for the test and training sets, respectively, from this dataset. Note that all of the photos have been evaluated by a radiologist, regardless of their reference.

It should be noted that images in this dataset have different resolutions, including high-resolution images, i.e., more than 1900×1400, and some low-resolution images, i.e., below 400×400. This is a positive point for the model evaluation because it can obtain a reasonable accuracy with variable imagery methodology and different image resolutions. In fact, if all the images have a high resolution, the model may achieve an acceptable result, but it certainly does not achieve acceptable results for real datasets with various resolution images. In this case, the results are actually biased. In other words, although it is desired to gather all COVID-19 images in completely controlled conditions, which causes super-clean and high-resolution images, It is not appropriate as the field of machine learning advances. Also, the COVID-19 images collected from various sources result in different dynamic ranges (also from ChexPert); therefore, In order to reduce the model's sensitivity to dynamic ranges during the training phase, all photos are scaled to the same distribution.

The name of the second dataset is the *COVIDetectioNet* dataset (Turkoglu, 2021), which is generated from publicly available X-rays. This dataset is a combination of three different chest X-ray datasets that were previously published on Kaggle and Github. This dataset includes 4290 chest X-rays of pneumonia, 219 COVID-19, and 1583 normal chest X-rays image. Table 1 provides detailed information about the resource datasets, and Table 2 lists the final datasets utilized in this investigation.

Typical images are displayed in Fig. 1 together with the appropriate marked areas. There are 2,000 training samples and 3,000 test samples in COVID-Xray-5 k. This dataset also includes COVID-19 positive cases, while the negative cases are drawn from a portion of the ChexPert dataset (Irvin et al., 2019).

4. Methodology

In this section, the searching agent of ChOA (i.e., chimps) and loss (fitness) function, which are the main concepts for introducing a problem for a metaheuristic algorithm, will be discussed.

4.1. Presentation of chimps

When utilizing optimization techniques to tune a deep network, there are ty-pically-two basic problems. The Chimps must first

accurately describe the parameters of the structure. The fitness function must then be defined in terms of the problem under consideration. A separate step in tuning a DCNN with ChOA is the presentation of the network parameters. As a result, in order to achieve the best detection accuracy, key DCNN parameters, such as the biases and connection - weights of FCL, should be precisely defined. To summarize, ChOA optimizes the weights and bias of the final layer, which is used to determine the fitness function for the loss function. Actually, the ChOA uses chimps to represent the bias and weight values from the final layer.

In general, the vector, matrix, and binary configurations are used to display the biases and weights of a DCNN as individuals of the *meta*-heuristic algorithms. The ChOA requires the parameters for a vector-based model, hence in this research, the individual is displayed in Eq. (12) and Fig. 2.

$$\boldsymbol{Chimps} = [W_{11}, W_{12}, ..., W_{nh}, b_1, ..., b_h, M_{11}, ..., M_{hm}] \tag{12}$$

In this equation, W_{ij} denotes the weight between the i_{th} input neuron and the j_{th} hidden node, n indicates the input neurons' number, b_j shows the j_{th} bias of hidden neurons, and *Mjo* denotes the weight from the j_{th} hidden to the o_{th} output neurons. As indicated previously, the suggested design consists of a straightforward LeNet-5 framework. In this section, two network structures, i.e., i-6c-2 s-12c-2 s and i-8c-2 s-16c-2 s, are utilized, in which the pooling and convolution layers are denoted by C and S, respectively. Also, t he kernel size of the convolution layer is 5x5, and the down sampling scale is 2.

4.2. Loss function

DCNN is trained using the ChOA algorithm (i.e., DCNN-ChOA) to achieve the best accuracy and reduce evaluated classification errors. In this regard, the loss function utilized in DCNN-ChOA is as follows:

$$y = \frac{1}{2}\sqrt{\frac{\sum_{i=0}^{N}(o-d)^2}{N}} \tag{13}$$

Where N indicates the number of training samples, d stands for the intended output, and o is the computed output. The ChOA has two termination criteria, either achieving maximum iteration or a preset loss function. Consequently, Fig. 3 exhibit the block diagram of DCNN-ChOA.

5. Simulation results and discussion

The effectiveness of the classifier was shown using ROC curves on each sample in the testing dataset. The probability of accurate detection is generally represented by the area under the ROC curve (AUC). LeNet-5, DCNN-GA, and MSAD are only a few of the benchmark models that are used to assess the effectiveness of DCNN-ChOA. The ROC and precision-recall curves for the i-6c-2 s-12c-2 s and i-8c-2 s-16c-2 s structures, respectively, are shown in Fig. 4a and b.

Training was repeated 10 times for a total of 5 to 12 min, and the developed DCNN-ChOA achieved a detection accuracy of 98.11 percent or higher on the validation dataset. Since there is such a large discrepancy between the outcomes, we utilize a weighted average of the Ten trained DCNN-ChOA and validate the accuracy of the weights to create an ensemble. The validation accuracy for the mixed ensemble DCNN-ChOA is 99.11 %. LeNet-5 DCNN obtained an accuracy between about 73.58 % and 87.31 % at the same time, while the resulting ensemble achieved a accuracy of 84.58 % on the validation dataset. These numbers demonstrate the remarkable detection performance of the DCNN-ChOA detector when compared to other benchmarks. The suggested DCNN-ChOA, for contrast, offers over 99.11 % accurate detection with less than 0.89 % false alarm rate. The precision-recall figure, in general, shows how recall and accuracy are traded off at different threshold values. Fig. 4a and b clearly indicate that DCNN-ChOA has a larger AUC than other models. As a result, compared to other benchmark detectors, it reveals a reduced rate of false negative and false positive results.

Fig. 5 displays the accuracy and Fig. 6 displays the computing time for the i-6c-2 s-12c-2 s structure. In Figs. 7 and 8, in descending order, are summarized the results for accuracy and computation time for the i-8c-2 s-16c-2 s structure. The simulations generally showed that the outcomes were improved with increasing epoch values. It should be mentioned that errorbars are used to depict the standard deviation (STD-DEV).

Finally, a comprehensive comparison between the DCNN-ChOA and other existing methods using the *COVID-Xray-5 k* dataset is tabulated in Table 7. The *COVID-Xray-5 k* introduced in (Minaee et al., 2020), which is the baseline dataset and method for the COVID-19 recognition task, achieved an average accuracy of 0.766 using the conventional DCNNs. Since most references have used the sensitivity, specificity, and accuracy metric to compare the results, this metric is used to compare the results of the proposed method with other benchmark methods.

As can be seen from the results of Table 7, the proposed model with structure i-2 s-8c-2 s-16c represents the best accuracy (i.e., 100 %), followed by the i-2 s-8c-2 s-16c structure and VGG19 with 99.38 % and 99.33 %, respectively. Of course, it should be noted that the 19-layer VGG 19 network is much more complex than the 5-layer LeNet-5.

The results of the simulation show that DCNN-ChOA achieves the best outcomes for practically all epochs. The DCNN-performance ChOA's gain over the DCNN changes with each epoch, with values ranging from 2.82 (the tenth epoch) to 5.94 (the first epoch). Taking into account the randomness of both ChOA and the connection weight of the fully-connected layer, the DCNN-ChOA takes from around 0.8619 times (for the first epoch, 88.01/102.11) to 08,147 times (for the tenth epoch, 923.43/1133.44) as long to compute as the LetNet-5. It is clear that the efficiency of the ChOA grows with the number of epochs because the stochastic character of the ChOA causes the complexity to decrease. Experts in data science might suggest that the optimal outcome should be shown in terms of the confusion matrix, total precision, accuracy, recall, ROC curve, etc. However, if the data cannot be comprehended, these optimal outcomes may not be adequate for medical specialists. Medical professionals and data scientists will have a deeper grasp of the network's decision-making process if the ROI driving that process can be identified.

In addition to ensuring classification accuracy, we look for features within an image that aid experts in correctly and easily classifying the images. This is accomplished through the use of class activation mapping (CAM) (Hu, Khishe, Mohammadi, Parvizi, Taher Karim, et al., 2021). As a result, by adding the DCNN model's probability to the final convolutional layer of the associated model, the distinct discriminative zones for each category are highlighted.

The activation map of the ReLU layer, which comes after the last convolution layer, creates the CAM for a particular image class. Each activation mapping's weighted average is used to calculate class grades. After the final convolutional layer, CAM introduces a cumulative average pooling layer that is utilized to generate connection weights based on geographic location. Therefore, it enables locating the exact regions within a photo that identify the class specificity before the softmax layer, which can improve trust in the results.

Fig. 9 is an example feature map for COVID19 and Non-COVID19 input images. Images that have been masked for COVID19 and Non-COVID19 are displayed in Fig. 10. Consequently, the picture discriminative regions for COVID19 and Non-COVID19 are displayed in Figs. 11 and 12, respectively. In fact, Figs. 11 and 12 depict the results of the CAM demonstration in the "COVID19″ and "Non-COVID19″ instances, respectively. This is confirmed by the suggested model, which also locates the optimal region for its selection based on a set of discriminating criteria.

In the COVID-19 cases, several regions are obviously emphasized (reddish color). This proves that the system successfully categorizes the

data. This visualization of deep learning techniques can help medical practitioners and radiologists understand these models from a different perspective and with greater depth.

6. Conclusion

An effective DCNN model for detecting Covid-19 X-rays was proposed in this study, and the ChOA was used in its development. On the COVIDetectioNet and COVID-Xray-5 k datasets, the developed detector was benchmarked. Two structures, i-6c-2 s-12c-2 s and i-8c-2 s-16c-2 s, were chosen for comparison after hyperparameter adjustment. The outcomes were contrasted with DCNN-GA, MSAD, and standard DCNN. Since there was such a large discrepancy between the outcomes, we used a weighted average of the ten trained DCNN-ChOA and the validation accuracy of the weights to create an ensemble. Validation accuracy was 99.11 % for the ensemble DCNN-ChOA. The final ensemble of LeNet-5 achieved an accuracy of 84.58 % in validation dataset. Comparatively, the suggested DCNN-ChOA produced over 99.11 % accuracy with a false alarm rate of less than 0.89 %. In addition to the previous comparison and in order to have a baseline, the results of the proposed fine-tuned models were compared to sixteen state-of-the-art classifiers, including ResNet18, ResNet50, SqueezeNet, DenseNet-121, ResNet-101, CB-STMRENet, VGG16, VGG19, OptiCNN, CNN, Deep Decision Tree, Support Vector Machine, Naïve Bayes algorithm, K-Nearest Neighbors, and Random Forest, which have been applied to the identical dataset, i.e., COVID-Xray-5 k. The findings showed that when compared to these well-known classifiers, the developed detector can deliver very competitive results. The possible COVID-19-infected areas were also identified using the CAM concept. Results showed that highlighted regions were completely connected with clinical outcomes, which was also supported by experts.

The following topics can be considered as future research direction: applying DCNN-ChOA for other image classification tasks, including breast or brain cancer diagnosis, sonar and radar image classification, and agricultural image recognition. Although DCNN-ChOA presented some merits, using a hybrid method, especially an iterative method like ChOA, leads to high complexity computation; therefore, some unsupervised or semi-supervised learning can help reduce time and space complexity. Recently some modifications of ChOA, including weighted ChOA (WChOA), Dynamic Levy flight ChOA (DLF-ChOA), etc., have been proposed for the various filed of optimization problems. So, the improved version of ChOA or other well-known metaheuristic optimizers like SMA, AOA, or MPA can be used for the DCNN fine-tuning task. Considering the fact that the more comprehensive data sets, the more robust results, using more extensive and more diverse datasets in future studies can lead to more robust results.

Declaration of Competing Interest

The authors declare that they have no known competing financial interests or personal relationships that could have appeared to influence the work reported in this paper.

Acknowledgments

We would also like to show our gratitude to Dr. Mehdi Ramezani for approving X-ray images, and we thank four anonymous reviewers for their so-called insights.

References

Afrakhteh, S., Mosavi, M. R., Khishe, M., & Ayatollahi, A. (2020). Accurate Classification of EEG Signals Using Neural Networks Trained by Hybrid Population-physic-based Algorithm. *International Journal of Automation and Computing*. https://doi.org/10.1007/s11633-018-1158-3

Ahammed, K., Satu, M. S., Abedin, M. Z., Rahaman, M. A., & Islam, S. M. S. (2020). *Early Detection of Coronavirus Cases Using Chest X-ray Images Employing Machine Learning and Deep Learning Approaches*. MedRxiv.

Arnal, J., Chillarón, M., Parcero, E., Súcar, L. B., & Vidal, V. (2020). A Parallel Fuzzy Algorithm for Real-Time Medical Image Enhancement. *International Journal of Fuzzy Systems, 22*(8), 2599–2612.

Asif, S., Wenhui, Y., Jin, H., Tao, Y., & Jinhai, S. (2020). Classification of COVID-19 from Chest Radiography Images Using Deep Convolutional Neural Network. *Journal of Xidian University*. https://doi.org/10.37896/jxu14.8/061

Ban, Y., Liu, M., Wu, P., Yang, B., Liu, S., Yin, L., & Zheng, W. (2022). Depth Estimation Method for Monocular Camera Defocus Images in Microscopic Scenes. *Electronics, 11*(13), 2012.

Barshooi, A. H., & Amirkhani, A. (2022). A novel data augmentation based on Gabor filter and convolutional deep learning for improving the classification of COVID-19 chest X-Ray images. *Biomedical Signal Processing and Control, 72*, Article 103326.

Cao, Z., Wang, Y., Zheng, W., Yin, L., Tang, Y., Miao, W., … Yang, B. (2022). The algorithm of stereo vision and shape from shading based on endoscope imaging. *Biomedical Signal Processing and Control, 76*, Article 103658.

Che Azemin, M. Z., Hassan, R., Mohd Tamrin, M. I., & Md Ali, M. A. (2020). COVID-19 deep learning prediction model using publicly available radiologist-adjudicated chest X-ray images as training data: preliminary findings. *International Journal of Biomedical Imaging, 2020*.

Chhikara, P., Tekchandani, R., Kumar, N., Chamola, V., & Guizani, M. (2020). DCNN-GA: A Deep Neural Net Architecture for Navigation of UAV in Indoor Environment. *IEEE Internet of Things Journal*. https://doi.org/10.1109/jiot.2020.3027095

Cohen, J. P., Morrison, P., Dao, L., Roth, K., Duong, T. Q., & Ghassemi, M. (2020). Covid-19 image data collection: Prospective predictions are the future. *ArXiv Preprint*. ArXiv:2006.11988.

Dai, B., Zhang, B., Niu, Z., Feng, Y., Liu, Y., & Fan, Y. (2022). A Novel Ultrawideband Branch Waveguide Coupler With Low Amplitude Imbalance. *IEEE Transactions on Microwave Theory and Techniques*.

Dansana, D., Kumar, R., Bhattacharjee, A., Hemanth, D. J., Gupta, D., Khanna, A., & Castillo, O. (2020). Early diagnosis of COVID-19-affected patients based on X-ray and computed tomography images using deep learning algorithm. *Soft Computing*, 1–9.

Fan, H., Zheng, L., Yan, C., & Yang, Y. (2018). Unsupervised person re-identification: Clustering and fine-tuning. *ACM Transactions on Multimedia Computing, Communications and Applications.*. https://doi.org/10.1145/3243316

Feng, Y., Zhang, B., Liu, Y., Niu, Z., Fan, Y., & Chen, X. (2022). *A D-band Manifold Triplexer With High Isolation Utilizing Novel Waveguide Dual-Mode Filters*. IEEE Transactions on Terahertz Science and Technology.

Hassan, B. A., Rashid, T. A., & Hamarashid, H. K. (2021). A novel cluster detection of COVID-19 patients and medical disease conditions using improved evolutionary clustering algorithm star. *Computers in Biology and Medicine, 138*, Article 104866.

Heidari, M., Mirniaharikandehei, S., Khuzani, A. Z., Danala, G., Qiu, Y., & Zheng, B. (2020). Improving the performance of CNN to predict the likelihood of COVID-19 using chest X-ray images with preprocessing algorithms. *International Journal of Medical Informatics, 144*, Article 104284.

Heidari, M., Mirniaharikandehei, S., Khuzani, A. Z., Danala, G., Qiu, Y., & Zheng, B. (2021). Detecting COVID-19 infected pneumonia from x-ray images using a deep learning model with image preprocessing algorithm. *Medical Imaging 2021: Computer-Aided Diagnosis*, *11597*, 115970V.

Hemdan, E.-E.-D., Shouman, M. A., & Karar, M. E. (2020). Covidx-net: A framework of deep learning classifiers to diagnose covid-19 in x-ray images. *ArXiv Preprint*. ArXiv: 2003.11055.

Hinton, G. E., & Salakhutdinov, R. R. (2006). Reducing the dimensionality of data with neural networks. *Science*. https://doi.org/10.1126/science.1127647

Hu, T., Khishe, M., Mohammadi, M., Parvizi, G.-R., Karim, S. H. T., & Rashid, T. A. (2021a). Real-time COVID-19 diagnosis from X-Ray images using deep CNN and extreme learning machines stabilized by chimp optimization algorithm. *Biomedical Signal Processing and Control, 102764*.

Hu, T., Khishe, M., Mohammadi, M., Parvizi, G. R., Taher Karim, S. H., & Rashid, T. A. (2021b). Real-time COVID-19 diagnosis from X-Ray images using deep CNN and extreme learning machines stabilized by chimp optimization algorithm. *Biomedical Signal Processing and Control, 68*, Article 102764. https://doi.org/10.1016/j.bspc.2021.102764

Irvin, J., Rajpurkar, P., Ko, M., Yu, Y., Ciurea-Ilcus, S., Chute, C., Marklund, H., Haghgoo, B., Ball, R., Shpanskaya, K., Seekins, J., Mong, D. A., Halabi, S. S., Sandberg, J. K., Jones, R., Larson, D. B., Langlotz, C. P., Patel, B. N., Lungren, M. P., & Ng, A. Y. (2019). CheXpert: A large chest radiograph dataset with uncertainty labels and expert comparison. *33rd AAAI Conference on Artificial Intelligence, AAAI 2019, 31st Innovative Applications of Artificial Intelligence Conference, IAAI 2019 and the 9th AAAI Symposium on Educational Advances in Artificial Intelligence, EAAI 2019*. https://doi.org/10.1609/aaai.v33i01.3301590.

Iwendi, C., Bashir, A. K., Peshkar, A., Sujatha, R., Chatterjee, J. M., Pasupuleti, S., … Jo, O. (2020). COVID-19 patient health prediction using boosted random forest algorithm. *Frontiers in Public Health, 8*, 357.

Jin, K., Yan, Y., Chen, M., Wang, J., Pan, X., Liu, X., … Ye, J. (2022). Multimodal deep learning with feature level fusion for identification of choroidal neovascularization activity in age-related macular degeneration. *Acta Ophthalmologica, 100*(2), e512. e520.

Khan, A. I., Shah, J. L., & Bhat, M. M. (2020). CoroNet: A deep neural network for detection and diagnosis of COVID-19 from chest x-ray images. *Computer Methods and Programs in Biomedicine, 196*, Article 105581.

Khan, I. U., & Aslam, N. (2020). A deep-learning-based framework for automated diagnosis of COVID-19 using X-ray images. *Information, 11*(9), 419.

Khishe, M., & Mosavi, M. R. (2019). Improved whale trainer for sonar datasets classification using neural network. *Applied Acoustics*. https://doi.org/10.1016/j.apacoust.2019.05.006

Khishe, M., & Mosavi, M. R. (2020). Chimp optimization algorithm. *Expert Systems with Applications*. https://doi.org/10.1016/j.eswa.2020.113338

Khishe, M., Caraffini, F., & Kuhn, S. (2021). Evolving Deep Learning Convolutional Neural Networks for early COVID-19 detection in chest X-ray images. *Mathematics, 9*(9), 1002.

LeCun, Y. (2015). LeNet-5, convolutional neural networks. *URL: Http://Yann. Lecun. Com/Exdb/Lenet, 20*(5), 14.

Li, J., Han, L., Zhang, C., Li, Q., & Liu, Z. (2022). Spherical Convolution empowered Viewport Prediction in 360 Video Multicast with Limited FoV Feedback. *ACM Transactions on Multimedia Computing. Communications*. and Applications (TOMM.

Li, Y., Du, L., & Wei, D. (2021). Multiscale CNN based on component analysis for SAR ATR. *IEEE Transactions on Geoscience and Remote Sensing*.

Liao, L., Du, L., & Guo, Y. (2021). Semi-Supervised SAR Target Detection Based on an Improved Faster R-CNN. *Remote Sensing, 14*(1), 143.

Lu, C., Liu, Q., Zhang, B., & Yin, L. (2022). A Pareto-based hybrid iterated greedy algorithm for energy-efficient scheduling of distributed hybrid flowshop. *Expert Systems with Applications, 117555*.

Luo, G., Yuan, Q., Li, J., Wang, S., & Yang, F. (2022a). Artificial intelligence powered mobile networks: From cognition to decision. *IEEE Network, 36*(3), 136–144.

Luo, G., Zhang, H., Yuan, Q., Li, J., & Wang, F.-Y. (2022b). ESTNet: Embedded Spatial-Temporal Network for Modeling Traffic Flow Dynamics. *IEEE Transactions on Intelligent Transportation Systems.*

Mansour, N. A., Saleh, A. I., Badawy, M., & Ali, H. A. (2021). Accurate detection of Covid-19 patients based on Feature Correlated Naïve Bayes (FCNB) classification strategy. *Journal of Ambient Intelligence and Humanized Computing*, 1–33.

Martens, J. (2010). Deep learning via Hessian-free optimization. *ICML 2010 – Proceedings, 27th International Conference on Machine Learning*.

Minaee, S., Kafieh, R., Sonka, M., Yazdani, S., & Jamalipour Soufi, G. (2020). Deep-COVID: Predicting COVID-19 from chest X-ray images using deep transfer learning. *Medical Image Analysis*. https://doi.org/10.1016/j.media.2020.101794

Mohammed, M. A., Abdulkareem, K. H., Al-Waisy, A. S., Mostafa, S. A., Al-Fahdawi, S., Dinar, A. M., … Alhakami, H. (2020). Benchmarking methodology for selection of optimal COVID-19 diagnostic model based on entropy and TOPSIS methods. *Ieee Access, 8*, 99115–99131.

Mosavi, M. R., Khishe, M., & Akbarisani, M. (2017a). Neural Network Trained by Biogeography-Based Optimizer with Chaos for Sonar Data Set Classification. *Wireless Personal Communications*. https://doi.org/10.1007/s11277-017-4110-x

Mosavi, M. R., Khishe, M., Hatam Khani, Y., & Shabani, M. (2017b). Training radial basis function neural network using stochastic fractal search algorithm to classify sonar dataset. *Iranian Journal of Electrical and Electronic Engineering*. https://doi.org/10.22068/IJEEE.13.1.10

Nilashi, M., Samad, S., Shahmoadi, L., Ahmadi, H., Akbari, E., & Rashid, T. A. (2020). The COVID-19 infection and the immune system: The role of complementary and alternative medicines. *Biomedical Research, 0970–938X*, 1–4.

Ozturk, T., Talo, M., Yildirim, E. A., Baloglu, U. B., Yildirim, O., & Rajendra Acharya, U. (2020). Automated detection of COVID-19 cases using deep neural networks with X-ray images. *Computers in Biology and Medicine*. https://doi.org/10.1016/j.compbiomed.2020.103792

Pan, D., Xia, X.-X., Zhou, H., Jin, S.-Q., Lu, Y.-Y., Liu, H., … Jin, Z.-B. (2020). COCO enhances the efficiency of photoreceptor precursor differentiation in early human embryonic stem cell-derived retinal organoids. *Stem Cell Research & Therapy, 11*(1), 1–12.

Qiao, W., Khishe, M., & Ravakhah, S. (2021). Underwater targets classification using local wavelet acoustic pattern and Multi-Layer Perceptron neural network optimized by modified Whale Optimization Algorithm. *Ocean Engineering, 219*, 108415. https://doi.org/https://doi.org/10.1016/j.oceaneng.2020.108415.

Rodriguez, A., Tabassum, A., Cui, J., Xie, J., Ho, J., Agarwal, P., … Prakash, B. A. (2020). *DeepCOVID: An Operational Deep Learning-driven Framework for Explainable Real-time COVID-19 Forecasting*. MedRxiv.

Rosa, G., Papa, J., Marana, A., Scheirer, W., & Cox, D. (2015). Fine-tuning convolutional neural networks using Harmony Search. *Lecture Notes in Computer Science (Including Subseries Lecture Notes in Artificial Intelligence and Lecture Notes in Bioinformatics)*. https://doi.org/10.1007/978-3-319-25751-8_82

Sarker, L., Islam, M. M., Hannan, T., & Ahmed, Z. (2020). *Covid-densenet: A deep learning architecture to detect covid-19 from chest radiology images*.

Shewchuk, J. R. (1994). *An introduction to the conjugate gradient method without the agonizing pain*. Department of Computer Science: Carnegie-Mellon University.

Tahir, H., Iftikhar, A., Mumraiz, M., & (2021). Forecasting COVID-19 via Registration Slips of Patients using ResNet-101 and Performance Analysis and Comparison of Prediction for COVID-19 using Faster R-CNN, Mask R-CNN, and ResNet-50. (2021). *International Conference on Advances in Electrical* (pp. 1–6). Communication and Sustainable Technologies (ICAECT): Computing.

Turkoglu, M. (2021). COVIDetectioNet: COVID-19 diagnosis system based on X-ray images using features selected from pre-learned deep features ensemble. *Applied Intelligence, 51*(3), 1213–1226.

Ucar, F., & Korkmaz, D. (2020). COVIDiagnosis-Net: Deep Bayes-SqueezeNet based diagnosis of the coronavirus disease 2019 (COVID-19) from X-ray images. *Medical Hypotheses, 140*, Article 109761.

Vinyals, O., & Povey, D. (2012). Krylov subspace descent for deep learning. *Journal of Machine Learning Research*.

Wang, L., Lin, Z. Q., & Wong, A. (2020). Covid-net: A tailored deep convolutional neural network design for detection of covid-19 cases from chest x-ray images. *Scientific Reports, 10*(1), 1–12.

Wong, H. Y. F., Lam, H. Y. S., Fong, A.-H.-T., Leung, S. T., Chin, T.-W.-Y., Lo, C. S. Y., … Chung, T.-W.-H. (2020). Frequency and distribution of chest radiographic findings in patients positive for COVID-19. *Radiology, 296*(2), E72. E78.

Wu, C., Khishe, M., Mohammadi, M., Karim, S. H. T., & Rashid, T. A. (2021). Evolving deep convolutional neutral network by hybrid sine–cosine and extreme learning machine for real-time COVID19 diagnosis from X-ray images. *Soft Computing*, 1–20.

Xie, Y., Sheng, Y., Qiu, M., & Gui, F. (2022). An adaptive decoding biased random key genetic algorithm for cloud workflow scheduling. *Engineering Applications of Artificial Intelligence, 112*, Article 104879.

Xu, Q., Zeng, Y., Tang, W., Peng, W., Xia, T., Li, Z., … Guo, J. (2020). Multi-task joint learning model for segmenting and classifying tongue images using a deep neural network. *IEEE Journal of Biomedical and Health Informatics, 24*(9), 2481–2489.

Yin, F., Xue, X., Zhang, C., Zhang, K., Han, J., Liu, B., … Yao, J. (2021). Multifidelity genetic transfer: An efficient framework for production optimization. *SPE J*, 1–22.

Yoo, S. H., Geng, H., Chiu, T. L., Yu, S. K., Cho, D. C., Heo, J., … Nhung, N. V. (2020). Deep learning-based decision-tree classifier for COVID-19 diagnosis from chest X-ray imaging. *Frontiers in Medicine, 7*, 427.

Zhang, K., Zhang, J., Ma, X., Yao, C., Zhang, L., Yang, Y., … Zhao, H. (2021). History Matching of Naturally Fractured Reservoirs Using a Deep Sparse Autoencoder. *SPE Journal*, 1–22.

Zhang, Y., Shi, X., Zhang, H., Cao, Y., & Terzija, V. (2022a). Review on deep learning applications in frequency analysis and control of modern power system. *International Journal of Electrical Power & Energy Systems, 136*, Article 107744.

Zhang, Z., Ma, P., Ahmed, R., Wang, J., Akin, D., Soto, F., … Demirci, U. (2022b). Advanced point-of-care testing technologies for human acute respiratory virus detection. *Advanced Materials, 34*(1), 2103646.

Zhang, Z., Liu, M., Zhou, M., & Chen, J. (2020). Dynamic reliability analysis of nonlinear structures using a Duffing-system-based equivalent nonlinear system method. *International Journal of Approximate Reasoning, 126*, 84–97.

Zhao, L., & Wang, L. (2022). A new lightweight network based on MobileNetV3. *KSII Transactions on Internet and Information Systems (TIIS), 16*(1), 1–15.

Zhou, W., Lv, Y., Lei, J., & Yu, L. (2019). Global and local-contrast guides content-aware fusion for RGB-D saliency prediction. *IEEE Transactions on Systems, Man, and Cybernetics: Systems*.

Zhu, B., Zhong, Q., Chen, Y., Liao, S., Li, Z., Shi, K., & Sotelo, M. A. (2022). A Novel Reconstruction Method for Temperature Distribution Measurement Based on Ultrasonic Tomography. *IEEE Transactions on. Ultrasonics*. Ferroelectrics, and Frequency Control.

Zhuo, Z., Wan, Y., Guan, D., Ni, S., Wang, L., Zhang, Z., … Lu, A. (2020). A loop-based and AGO-Incorporated virtual screening model targeting AGO-Mediated miRNA–mRNA interactions for drug discovery to rescue bone phenotype in genetically modified Mice. *Advanced Science, 7*(13), 1903451.

Zivkovic, M., Venkatachalam, K., Bacanin, N., Djordjevic, A., Antonijevic, M., Strumberger, I., & Rashid, T. A. (2021). Hybrid Genetic Algorithm and Machine Learning Method for COVID-19 Cases Prediction. *Proceedings of International Conference on Sustainable Expert Systems: ICSES, 2020*(176), 169.